ELSEVIER

Journal of Neuroscience Methods xxx (2006) xxx–xxx

JOURNAL OF NEUROSCIENCE METHODS

www.elsevier.com/locate/jneumeth

Determination of dominant simulated spindle frequency with different methods

Eero Huupponen [a,*], Wim De Clercq [b], Germán Gómez-Herrero [a], Antti Saastamoinen [a], Karen Egiazarian [a], Alpo Värri [a], Bart Vanrumste [b], Anneleen Vergult [b], Sabine Van Huffel [b], Wim Van Paesschen [b], Joel Hasan [c], Sari-Leena Himanen [c]

[a] *Institute of Signal Processing, Tampere University of Technology, Korkeakoulunkatu 1, FIN-33101, Tampere, Finland*
[b] *Department of Electrical Engineering ESAT-SCD, Katholieke Universiteit Leuven, B-3001, Leuven, Belgium*
[c] *Department of Clinical Neurophysiology, Tampere University Hospital, P.O. Box 2000, Tampere, Finland*

Received 6 October 2005; received in revised form 2 December 2005; accepted 19 January 2006

Abstract

Accurate analysis of EEG sleep spindle frequency is challenging. The frequency content of true sleep spindles is not known. Therefore, simulated spindle activity was studied in the present work. Five types of simulated test signals were designed, all containing a dominant spindle represented by a 13-Hz sine wave as such or with a waxing and waning pattern accompanied by a secondary spindle activity in three test signals. Background EEG was included in four test signals, modeled either as small additional sinusoids across the spindle frequency range or as filtered Gaussian noise segments. The purpose of this study was to investigate how accurately the dominant spindle frequency of 13 Hz could be resolved with different methods in the presence of the interfering waveforms. A matching pursuit (MP) based approach, discrete Fourier transform (DFT) with Hanning windowing with and without zero padding, Hankel total least squares (HTLS) and wavelet methods were compared in the analyses. MP method provided best overall performance, followed closely by DFT with zero padding. Comparative studies like this are important to decide the method of choice in clinical sleep EEG analysis.
© 2006 Elsevier B.V. All rights reserved.

Keywords: Sleep EEG; Sleep spindles; Frequency analysis; DFT; Matching pursuit; Hankel total least squares; Wavelet

1. Introduction

Computer-based sleep analysis methods aim at providing a reproducible and accurate description of sleep process and sleep micro-events, as described, for instance, by Hasan (1996) as well as Penzel and Conradt (2000). Sleep spindles with frequencies ranging from 10.5 to 16 Hz are seen in sleep EEG with a typical duration of 0.5–2.0 s occurring with highest density in fairly light sleep and with lower density in deep sleep. Spindles are one of the most important sleep micro-events. As reported by Naitoh et al. (1982) and Jankel and Niedermeyer (1985), spindles are considered sleep-maintaining events blocking the transfer of sensory information into the cerebral cortex at the level of thalamus. In this state of reduced sensory activation, sleep related brain processes occur. Furthermore, sleep EEG is quite different from EEG during wakefulness. The sleep EEG oscillations generated in thalamo-cortical or cortico-cortical networks are typically of sinusoidal nature, for instance, sleep spindles, alpha activity and also much of delta activity.

Clearly, frequency analysis of short EEG events like spindles (Fig. 1) is very challenging as the frequency resolution should be as high as possible. Wavelet-based method for spindle detection has been presented by Akin and Akgül (1998). Matching pursuit approach was applied to spindle detection and frequency analysis by Zygierewicz et al. (1999). That work gives an excellent presentation of MP approach in spindle detection, also comparing automatic spindle detections to expert scorings. Our previously developed automatic spindle analysis method made use of DFT-based features in spindle detection and DFT in subsequent spindle frequency analysis (Huupponen et al., 2000, 2003). MP-based approach was applied to spindle frequency analysis of spindles detected based on combination of their amplitude and DFT-based features (Huupponen et al., 2005a). Recently, we compared DFT and MP methods in spindle

* Corresponding author. Tel.: +358 3 3115 3858; fax: +358 3 3115 3087.
E-mail address: eero.huupponen@tut.fi (E. Huupponen).

0165-0270/$ – see front matter © 2006 Elsevier B.V. All rights reserved.
doi:10.1016/j.jneumeth.2006.01.013

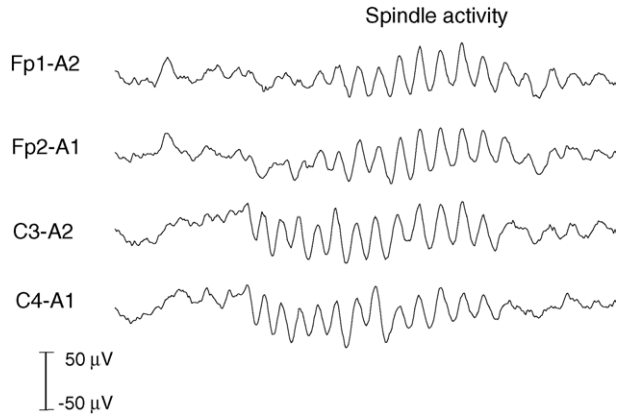


Fig. 1. Two seconds of true sleep EEG signals. Clear spindle activity is seen on all four channels.

frequency determination in EEG signal segments, which were visually marked as spindles by a sleep expert (Huupponen et al., 2005b). In that study it became obvious that the spindle frequency values provided by the two methods could be compared to each other, but unfortunately, there was no way of knowing which method provided results closest to the true spindle frequencies.

None of the above mentioned studies could assess the accuracy of spindle frequency determination. This is because the true frequency of a true EEG spindle cannot be known. Therefore, simulated test signals need to be used. The present work was designed so that the spindle frequency values determined by different methods could be quantitatively compared as the dominant spindle frequency was known to be 13 Hz in all test signals. Thus, the present work can be seen as comparison of frequency analysis methods applied to artificial sleep EEG segments representing spindles that have been visually marked by a sleep expert. Alternatively, one can see this so that the simulated signal segments represent spindles that have been detected by any automatic method presented previously, for example, by Schimicek et al. (1994), Zygierewicz et al. (1999), or Huupponen et al. (2000, 2005a).

To the best of our knowledge, Hankel total least squares (HTLS, Lemmerling, 1999; Van Huffel et al., 1994) has never been applied for spindle frequency analysis. However, HTLS has previously been applied with success in NMR spectroscopy (Van Huffel et al., 1994), EEG signal processing (De Clercq et al., 2004), in vivo near infrared spectra and blood pressure (Morren et al., 2002).

Spindle frequency typically slows down along with deepening sleep and increases as the sleep gets lighter inside sleep cycles, as reported by Himanen et al. (2002). Sleep spindles occurring in frontal brain regions have been reported to be generally of lower frequency than those in central brain regions (Zeitlhofer et al., 1997; Zygierewicz et al., 1999; Himanen et al., 2002). Night-to-night variation of spindles in different age groups was studied by Gondenck and Smith (1974) where the spindle frequency characteristics seemed to be relatively stable during the two nights studied. The spindle frequency may stay slower in disturbed sleep as was the case with apnea patients as compared to healthy subjects in a recent work by Himanen et al. (2003). Knowledge about the clinical meaning of sleep spindles is continuously growing and spindles are also seen in anesthesia EEG. As precise as possible determination of spindle frequency is important so that the clinical use of automatic EEG analysis methods is of as high-quality as possible. The objective of the present work was to quantitatively compare determination of simulated spindle frequencies applying five methods, namely matching pursuit-based approach, DFT with Hanning windowing with and without zero padding, wavelets and HTLS.

2. Materials and methods

2.1. Test signal composition

The real-life dominant spindle activity is always accompanied by some level of background EEG waveforms, even within the relatively narrow frequency range of sleep spindles from 10.5 to 16 Hz. This background activity seems to be mostly of magnitude of 0.05–0.2 as compared to the dominant spindle activity based on our experience and also other studies (Werth et al., 1997; Uchida et al., 1994). In addition to this, it has recently been found that in about 5–10% of spindles the dominant spindle activity waveform is accompanied by a secondary relatively large spindle activity (Zygierewicz et al., 1999; Huupponen et al., 2005b).

The present test signals were designed for studying frequency determination of dominant 13 Hz spindle activity in test signal segments each known to contain a spindle. The study was focused on the frequency range of the spindles (10.5–16 Hz), so the artificial signals can be thought as modeling band-pass filtered sleep EEG segments. Five types of test signals were studied, denoted as A–E. The duration of every test signal was 0.5 s, equal to 128 signal samples with the considered sampling rate of 256 Hz.

2.1.1. Set I

2.1.1.1. Test signals A: the dominant spindle activity and six background EEG sinusoids superimposed. In test signals A, the dominant spindle activity was accompanied by six smaller sinusoids representing the background EEG in the spindle frequency range. The test signal segments, denoted as $s_{\mathrm{EEG},k}\{i\}$, were of the form

$$s_{\mathrm{EEG},k}\{i\} = \cos\{2\pi f_{\mathrm{dom_spin}} i\Delta t\} + \gamma\sum_{j=1}^{6}\cos\{2\pi f_{\mathrm{backg},j} i\Delta t + \varphi_{k,j}\},$$

$$i = 0, 1, \ldots, 127, \quad k = 1, 2, \ldots, 56,$$

where k is the test signal number and i is the signal sample number. The frequency of the dominant spindle activity, denoted as $f_{\mathrm{dom_spin}}$, was 13 Hz and Δt was the sampling interval. The relative amplitude of background sinusoids, denoted as γ, was set to 0.1 and their frequencies, denoted as $f_{\mathrm{backgr},j}$, ranged from 10.5 to 15.5 Hz in steps of 1 Hz. The random phase shifts $\varphi_{k,j}$ of uniform distribution between 0 and 2π rad (0.1π rad resolution) made each test signal sequence $s_{\mathrm{EEG},k}\{i\}$ different. These test

signals contained noticeable distortions to the appearance of the pure dominant spindle activity, although only the relatively small background activities were added.

2.1.1.2. Test signals B: the dominant spindle activity and band-pass filtered noise of 10.5–16 Hz. These were like test signals A, except that the background EEG was modeled as a filtered Gaussian noise signal. The simulated signal segments were of the form

$$s_{\mathrm{EEG},k}\{i\} = \cos\{2\pi f_{\mathrm{dom_spin}} i\Delta t\} + \eta n_k\{i\},$$
$$i = 0, 1, \ldots, 127, \quad k = 1, 2, \ldots, 56,$$

where $f_{\mathrm{dom_spin}}$ was 13 Hz and η was set to 0.3. The noise segments, denoted as $n_k\{i\}$, were formed by generating Gaussian noise of unit variance and then filtering them with a finite impulse response (FIR) filter of 401 taps with a pass band from 10.5 to 16.0 Hz, with −3 dB points at 9.9, 16.6 Hz and attenuation of at least 60 dB in the stop bands, and the amplitude level of $n_k\{i\}$ was scaled to be the same as the cosines.

2.1.1.3. Test signals C: the dominant and another simultaneous spindle activity superimposed. Test signals C imitated spindles which are composed of two spindle activities, but free of background EEG. The signal segments were of the form

$$s_{\mathrm{EEG},k}\{i\} = \cos\{2\pi f_{\mathrm{dom_spin}} i\Delta t\} + \beta\cos\{2\pi f_{\mathrm{other_spin},k} i\Delta t + \xi_k\},$$
$$i = 0, 1, \ldots, 127, \quad k = 1, 2, \ldots, 56,$$

where $f_{\mathrm{dom_spin}}$ was 13 Hz while the frequency of the other spindle, denoted as $f_{\mathrm{other_spin},k}$, ranged from 10.5 to 16 Hz in steps of 0.1 Hz. The random phase shift, denoted as ξ_k, was variable between test signals but kept constant in testing different relative amplitude values $\beta = 0.3$ and $\beta = 0.6$ in parallel.

2.1.1.4. Test signals D: the dominant and another simultaneous spindle activity and six backgound EEG sinusoids superimposed. Test signals D were like signals C with the background sinusoids added. The simulated signal segments were of the form

$$s_{\mathrm{EEG},k}\{i\} = \cos\{2\pi f_{\mathrm{dom_spin}} i\Delta t\} + \beta\cos\{2\pi f_{\mathrm{other_spin},k} i\Delta t + \xi_k\} + \gamma\sum_{j=1}^{6}\cos\{2\pi f_{\mathrm{backg},j} i\Delta t + \varphi_{k,j}\},$$
$$i = 0, 1, \ldots, 127, \quad k = 1, 2, \ldots, 56,$$

where $f_{\mathrm{dom_spin}}$ was 13 Hz and other waveform parameters β, γ, $f_{\mathrm{other_spin},k}$, ξ_k and $\varphi_{k,j}$ were corresponding to previous test signals.

2.1.1.5. Test signals E: the dominant and another simultaneous spindle activity and band-pass filtered noise of 10.5–16 Hz. These were like test signals D, except that the background EEG was modeled as a noise signal. The simulated signal segments were of the form

$$s_{\mathrm{EEG},k}\{i\} = \cos\{2\pi f_{\mathrm{dom_spin}} i\Delta t\} + \beta\cos\{2\pi f_{\mathrm{other_spin},k} i\Delta t + \xi_k\} + \eta n_k\{i\},$$
$$i = 0, 1, \ldots, 127, \quad k = 1, 2, \ldots, 56,$$

where $f_{\mathrm{dom_spin}}$ was 13 Hz and other waveform parameters β, η, $f_{\mathrm{other_spin},k}$ and ξ_k were corresponding to previous test signals. The noise segments $n_k\{i\}$ were formed similarly as in test signals B.

As a final step, all test signals of types A–E, were scaled to unity mean nominal amplitude as $\sum_{i=0}^{127}\frac{|s_{\mathrm{EEG},k}\{i\}|}{128} = 1$. This scaling was readily done to have constant amplitude levels, needed in some of the applied methods. Examples of test signals are seen in (Fig. 2).

2.1.2. Set II

A second set of test signals was determined so that the amplitude envelope of the dominant spindle was modulated to have the so-called waxing and waning spindle pattern. Gaussian distribution function, denoted as $G(x)$, was used to achieve this

$$G(x) = \frac{1}{\sigma\sqrt{2\pi}}\,\mathrm{e}^{(-(x-\mu)^2/2\sigma^2)}.$$

The modulating function, denoted as $a\{\mathrm{i}\}$, was determined so that it formed a complete waxing and waning pattern by selecting

$$a\{i\} = G((i+2)\times 0.015), \quad \mu = 1 \text{ and } \sigma = 0.32,$$
$$i = 0, 1, \ldots, 127.$$

To obtain test signal set II, in all test signals A–E, the dominant spindle activity, $\cos\{2\pi f_{\mathrm{dom_spin}} i\Delta t\}$, was replaced by $a\{i\}\times\cos\{2\pi f_{\mathrm{dom_spin}} i\Delta t\}$, $i = 0, 1, \ldots, 127$. The amplitude level of which was scaled to be the same as the pure cosine.

2.2. Frequency analysis methods

2.2.1. Matching pursuit-based method

The first method was based on the matching pursuit (MP) algorithm introduced by Mallat and Zhang (1993). Let $\varphi_\kappa\{i\}$, $i = 0, 1, \ldots, 127$, be a dictionary of code vectors of 128 samples (0.5 s), with κ being the indexing parameter of the dictionary. A decomposition of signal segment $s_{\mathrm{EEG},k}\{i\}$ using m code vectors of the dictionary can be presented as

$$s_{\mathrm{EEG},k}\{i\} = \sum_{j=1}^{m}\alpha_\kappa^{(j)}\varphi_\kappa^{(j)}\{i\} + R^{(m)}\{i\}, \quad i = 0, 1, \ldots, 127,$$

where $\alpha_\kappa^{(j)}$ is the expansion coefficient of code vector $\varphi_\kappa^{(j)}$ at jth iteration step, and $R^{(m)}$ is the residual signal. MP is an iterative algorithm to find such a decomposition that chooses at each iteration step the waveform in the dictionary that is best adapted to approximate the signal. Since we wanted only to determine the dominant frequency of the spindle, we used a MP decomposition

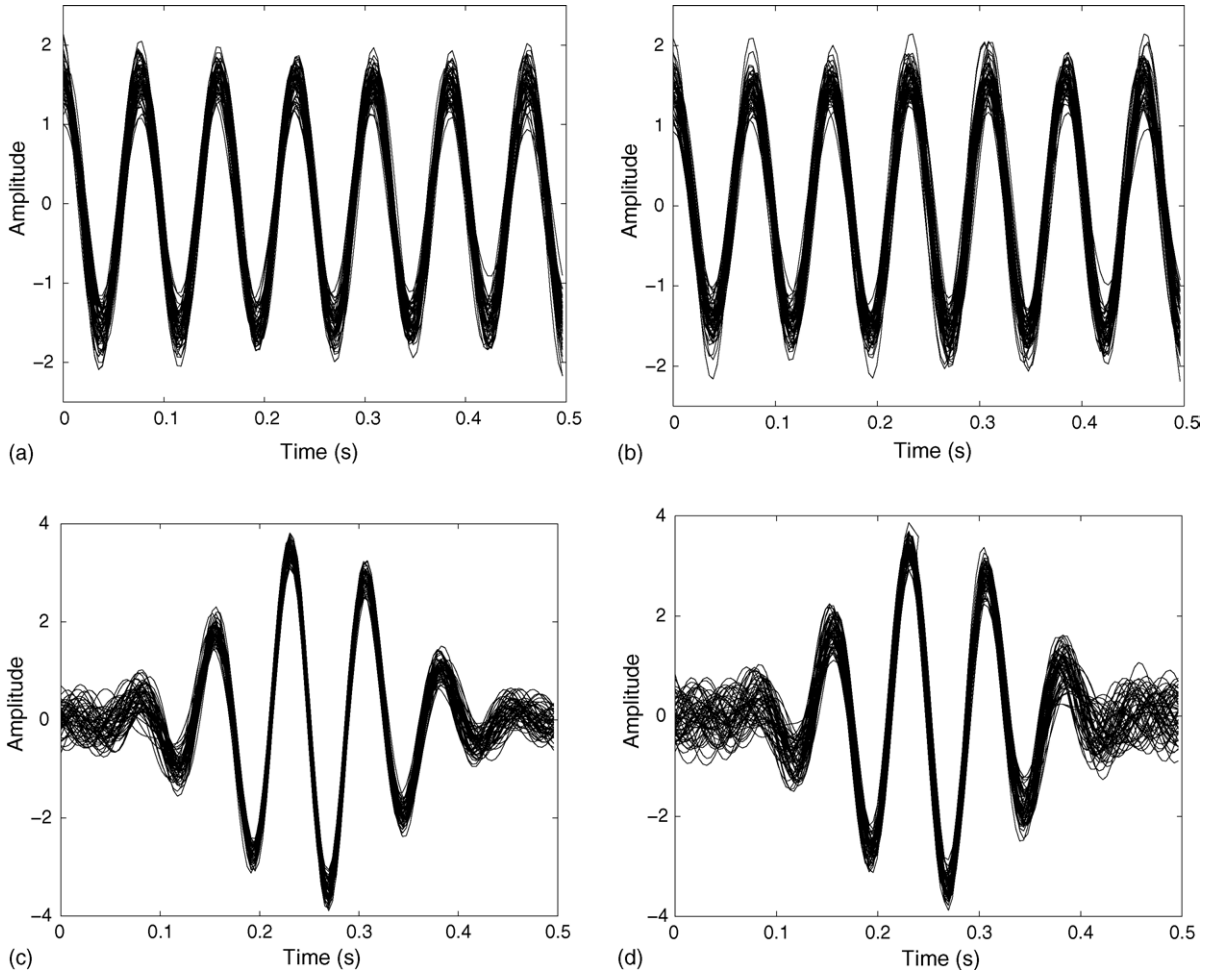


Fig. 2. Examples of simulated test signals $s_{\mathrm{EEG},k}$, $k = 1, 2, \ldots, 56$, of type B (a) and D (b) of set I and A (c) and E (d) of set II, β was 0.6 in (b) and (d). These panels show how the 13-Hz dominant spindle waveform varied due to the interfering waveforms.

into a single waveform, i.e. $m = 1$. The dictionary of code vectors consisted of pure sinusoidal code vectors

$$\varphi_\kappa\{i\} = \cos\{2\pi f i \Delta t + \psi\}, \quad i = 0, 1, \ldots, 127,$$

where f and ψ index the frequency and the phase shift of the cosine. We selected f to range from 10.5 to 16.0 Hz with 0.1 Hz frequency resolution. The phase shift ψ ranged from 0 to 2π in 20 divisions.

The set of MP code vectors was appended with amplitude-modulated versions with same range of parameters as

$$\varphi_\kappa\{i\} = a\{i\} \times \cos\{2\pi f i \Delta t + \psi\}, \quad i = 0, 1, \ldots, 127,$$

where $a\{i\}$ was the same Gaussian envelope as above.

A total of 2240 code vectors were obtained this way. They were normalized as

$$\sum_{i=0}^{127} \frac{|\varphi_\kappa\{i\}|}{128} = 1, \quad \kappa = 1, \ldots, 2240.$$

Examples of these code vectors are shown in Fig. 3a and b.

To estimate the dominant simulated spindle frequency, the test signal segment $s_{\mathrm{EEG},k}\{i\}$ was compared to each of the 2240 code vectors $\varphi_\kappa\{i\}$ by computing the respective squared Euclidean distances d:

$$d = \sum_{i=0}^{127} (\varphi_\kappa\{i\} - s_{\mathrm{EEG},k}\{i\})^2, \quad \kappa = 1, \ldots, 2240.$$

The overall minimum distance d indicated the code vector with best match to current spindle and the spindle frequency, denoted as $f_{\mathrm{MP}}[k]$ for the test signal k, was obtained as the frequency f of that code vector.

2.2.2. Discrete Fourier transform (DFT), rectangular and Hanning window

Also DFT-based spindle frequency estimates were determined. We used Hanning windowing of 128 samples (0.5 s). A windowed test signal segment was used as such and as zero-padded to the length of 2560 samples. DFT was taken from these sequences and the frequency resolution of the amplitude spectrum without zero padding was 2.0 Hz and with zero padding it was 0.1 Hz, same as in the MP analysis. Hanning windowing emphasized the central part of the signal segment providing a wide main lobe with dampened side lobes in the amplitude

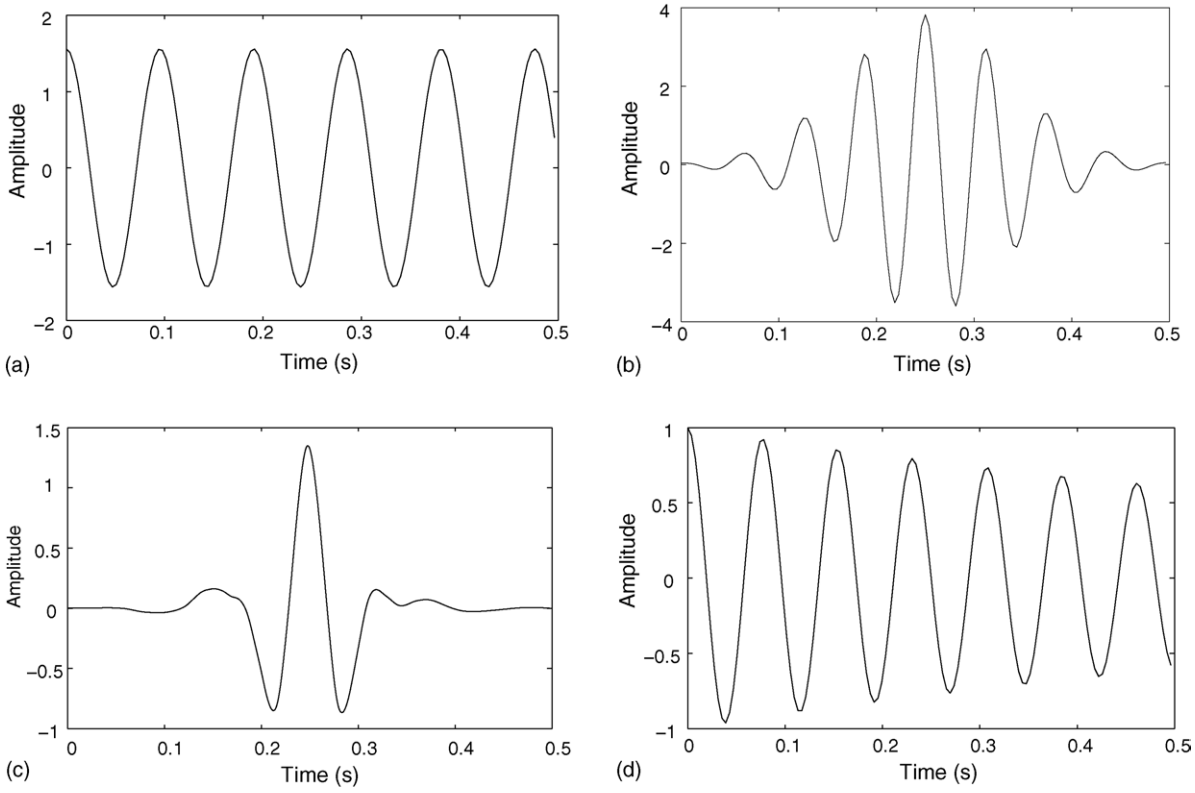


Fig. 3. Examples of the code vectors used. A pure and an amplitude modulated sinusoid of MP method with $f = 10.5$ Hz (a) and $f = 16.0$ Hz (b), $\varphi = 0$ rad in both. A mother wavelet of wavelet method (c) and an exponentially damped sinusoid of HTLS method with $f = 13.0$ Hz, $d = 1$, $a = 1$, $\varphi = 0$ rad (d).

spectrum. The estimated frequency of dominant spindle activity for a test signal $s_{\mathrm{EEG},k}\{i\}$ was determined as the frequency of the highest spectral peak, denoted as $f_{\mathrm{Han}}[k]$ or $f_{\mathrm{no}}[k]$, for zero padded version and with no zero padding, respectively.

2.2.3. Wavelet

We also tested the performance of the proposed matching pursuit procedure when using a Symmlet 8 wavelet packet (WP) dictionary. Wavelet packets are known to have good time–frequency localization properties and to be efficiently implemented in terms of filter banks. Wavelet packets produce a multi-resolution decomposition of the signal. In each level of this decomposition the tiling of the time–frequency plane is different and ranges from the Dirac's tiling (temporal representation of a signal) in the first level of the decomposition to Fourier's tiling (frequency representation) in the deepest possible decomposition level. In between, the time–frequency plane is divided in tiles well localized both in time and frequency. The frequency width of those tiles at level j is roughly

$$\Delta f = \frac{f_{\mathrm{s}}}{2^{j+1}}, \quad j = 0, \ldots, \log_2(n),$$

where n is the length of the signal being analyzed in samples and f_{s} is the sampling frequency. The width in temporal samples of the tiles at level j is approximately $\Delta t = 2^j$, for $j = 0, \ldots, \log_2(n)$. Therefore, the time and frequency support of the wavelet packet waveforms at each level of the decomposition are inversely proportional to each other. The finest frequency resolution

$$\Delta f = \frac{f_{\mathrm{s}}}{2n} = 1.0\,\mathrm{Hz} \text{ is obtained at level } \; j = \log_2(n),$$
$$\text{with } n = 128 \;\text{ and }\; f_{\mathrm{s}} = 256\,\mathrm{Hz}.$$

The dominant spindle frequency $f_{\mathrm{WP}}[k]$ was obtained as the central frequency, denoted as f_0, of the best matching WP waveform. The best matching WP waveform was the one having highest correlation with the spindle. Contrary to the DFT methods, the resolution of this estimated WP frequency depended on the level of the decomposition to which the best matching WP waveform belonged. At level j, the central frequencies of the WP waveforms (i.e. the possible values for f_0) are given by

$$f_0 = \frac{(k + 1/2)}{2^j}\frac{f_s}{2}, \quad k = 0, 1, \ldots, 2^j - 1.$$

Fig. 3c illustrates a mother wavelet.

2.2.4. Hankel total least squares (HTLS)

Yet another way to analyse the signals is to quantify them in the time domain by means of model-based (or parametric) methods. HTLS (Lemmerling, 1999; Van Huffel et al., 1994) is a subspace-based parametric method quantifying the parameters of signals, which are assumed to be modeled as a sum of exponentially damped sinusoids (EDS). When the EDS model fits the data, HTLS allows quantifying the frequencies accurately with fewer data points than non-parametric methods such as an

FFT. In HTLS the signal is modeled as a sum of K exponentially damped sinusoids:

$$y\{i\} = \sum_{k=1}^{K} a_k \exp(j\phi_k) \exp((-d_k + j2\pi f_k) i\Delta t),$$
$$i = 0, 1, \ldots, 127,$$

where $y\{i\}$ represents the ith modeled data point, $j = \sqrt{-1}$ and Δt is the constant sampling interval. The parameters to be determined are the frequencies f_k, the damping factors d_k, the amplitudes a_k and the phases φ_k. The model is a good approximation of the signal if the model-order K, which is twice the number of frequency components, is chosen correctly. The model order estimator described in (Papy et al., 2005) was used to estimate K. This model order estimator exploits the shift-invariance of the dominant subspace of the Hankel data matrix and does not require a threshold setting and penalization terms. The energy of each exponentially damped sinusoid was calculated as follows:

$$E\{k\} = \sum_{i=0}^{127} |a_k \exp(j\phi_k) \exp((-d_k + j2\pi f_k) i\Delta t)|^2,$$
$$k = 1, \ldots, K.$$

The frequency f_k of the exponentially damped sinusoid with the highest energy was used as the $f_{\mathrm{HTLS}}[k]$ for a test signal k. An example of an exponentially damped sinusoid is shown in Fig. 3d.

2.3. Method comparison

Statistical analysis of the dominant spindle frequency values provided by the five methods was done with two-sample Kolmogorov–Smirnov (K–S) test. This test requires that the two samples to be compared are statistically independent but does not make any other assumptions on the form of the two distributions unlike, for example, Mann–Whitney U-test and the ordinary t-test (Siegel, 1956). Significance level of 0.05 was used.

There were a total of 10 pair-wise K–S comparisons between distributions of spindle frequency values of $f_{\mathrm{MP}}[k]$, $f_{\mathrm{Han}}[k]$, $f_{\mathrm{no}}[k]$, $f_{\mathrm{WP}}[k]$ and $f_{\mathrm{HTLS}}[k]$, $k = 1, \ldots, 56$ per each test signal version.

In order to quantify the performance of each method, the mean error, denoted as $\bar{\Delta}$, of the estimated dominant spindle frequency value as compared to the ideal output of 13.0 Hz was formed as

$$\bar{\Delta} = \sum_{k=1}^{N} \frac{|f[k] - 13|}{N},$$

where $N = 56$ and $f[k] = f_{\mathrm{MP}}[k]$, $f_{\mathrm{Han}}[k]$, $f_{\mathrm{no}}[k]$, $f_{\mathrm{WP}}[k]$ and $f_{\mathrm{HTLS}}[k]$.

Also, to explore the level of confusion in waveform fitting, confusion, denoted as $c[k]$, was determined as

$$c[k] = \frac{d_{\min}}{\sum_{i=0}^{127} (c_{\min}[i])^2}, \quad \text{where } k = 1, \ldots, 56,$$

where $d_{\min}$ indicates the squared Euclidian distance of the best fitting code vector and $c_{\min}$ denotes the respective code vector. In DFT methods, the best fitting sinusoid was obtained based on amplitude and phase spectra. The values of $c[k]$ could exceed one especially if the estimated phase was off by much.

The mean confusion, denoted as $\bar{c}$, was also determined,

$$\bar{c} = \sum_{k=1}^{N} \frac{c[k]}{N},$$

where $N = 56$ and $c[k] = c_{\mathrm{MP}}[k]$, $c_{\mathrm{Han}}[k]$, $c_{\mathrm{no}}[k]$, $c_{\mathrm{WP}}[k]$ and $c_{\mathrm{HTLS}}[k]$, representing the confusion values.

3. Results

We generated 100 Monte-Carlo realizations of the 56 instances of the five types of test signals in sets I and II to assess the performance of the compared methods. Fig. 4 illustrates one of the 100 simulations with test signals of type B of set I. The results are summarized in Tables 1 and 2.

As there were ten statistical comparisons per each Monte-Carlo realization per each line of Table 1, we summarize the outcome here. In each Monte-Carlo realization we studied with K–S test if the distributions of estimated spindle frequency val-

Table 1
Mean error $\bar{\Delta}$ (Hz) and confusion $\bar{c}$ of dominant spindle frequency determination of set I, median values resulting from 100 Monte-Carlo realizations are given

Test signal type, additional components	β	Matching pursuit		DFT, Hanning windowing and zero padding		DFT, Hanning windowing and no zero padding		Wavelet		HTLS	
		$\bar{\Delta}$	$\bar{c}$	$\bar{\Delta}$	$\bar{c}$	$\bar{\Delta}$	$\bar{c}$	$\bar{\Delta}$	$\bar{c}$	$\bar{\Delta}$	$\bar{c}$
A, SinBack	–	0.08	0.04	0.13	0.04	1.0	1.95	1.49	0.74	**0.15E−4**	0.05
B, NoiseBack	–	**0.07**	0.03	0.11	0.04	1.0	1.92	1.52	0.75	0.08	0.04
C, OtherSpi	0.3	0.09	0.05	0.16	0.06	1.0	1.90	1.46	0.71	**3.5E−14**	0.07
C, OtherSpi	0.6	0.24	0.17	0.34	0.22	1.0	1.96	1.28	0.63	**3.6E−14**	0.28
D, OtherSpi + SinBack	0.3	0.14	0.08	0.21	0.10	1.0	1.98	1.41	0.68	**0.03**	0.13
D, OtherSpi + SinBack	0.6	0.26	0.20	0.37	0.33	1.0	2.12	1.29	0.62	**0.05**	0.33
E, OtherSpi + NoiseBack	0.3	0.13	0.08	0.20	0.09	1.0	1.99	1.41	0.69	**0.12**	0.10
E, OtherSin + NoiseBack	0.6	0.26	0.19	0.36	0.30	1.0	2.07	1.28	0.62	**0.16**	0.25

All test signals A–E contained the dominant spindle activity of 13 Hz. Additional signal components were sinusoidal background, noise background, other spindle and combinations of these, β is the relative magnitude of the other spindle activity. The smallest mean error in each test signal type is marked in bold.

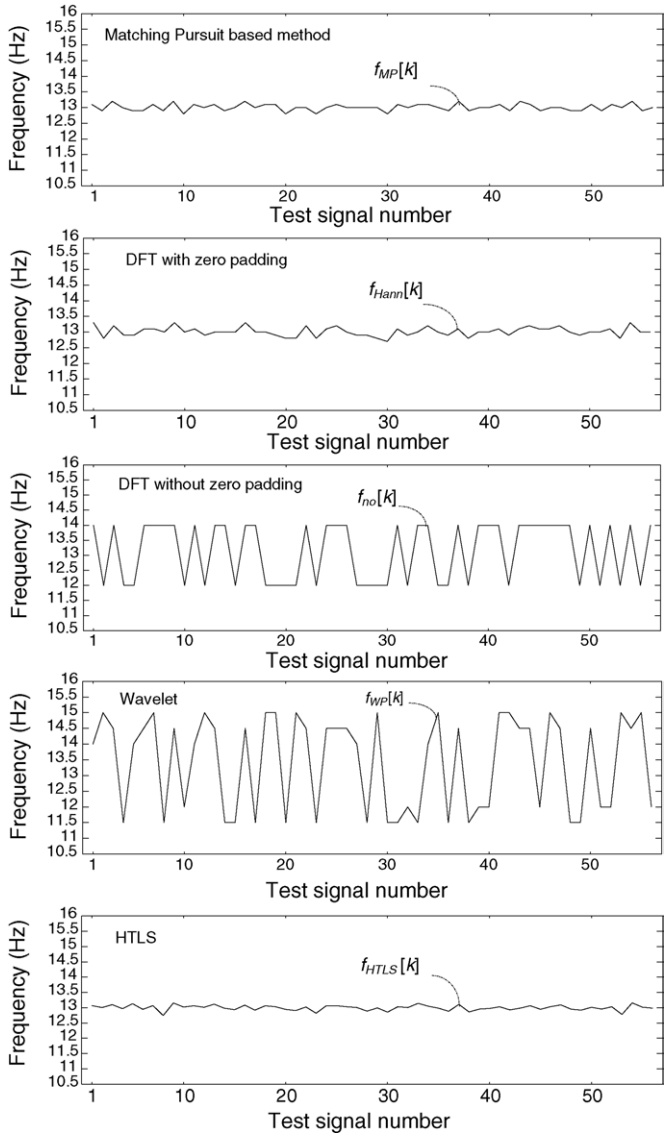


Fig. 4. Outcome of the dominant spindle frequency analyses in one of the 100 realizations of test signals of type B of set I. If a method would work ideally, the determined dominant spindle frequency values would be 13.0 Hz in each of the 56 instances. MP estimates of dominant spindle frequency are seen in the top panel, the DFT estimates are seen in the second and third panels, followed by wavelet and HTLS estimates. The mean error $\bar{\Delta}$ values in this realization were 0.08, 0.11, 1.0, 1.50 and 0.07 Hz, respectively.

ues between pairs of two methods were statistically significantly different, on–off. Based on the 100 realizations, if their median indicated difference, it is reported in the following.

Consider first the test signal set I where the envelope of spindle amplitude was constant. In test signals A and B, the distributions of dominant spindle frequency values of all methods were different from each other. In test signals C, the outcome was mostly the same, except for the distributions of $f_{\mathrm{MP}}[k]$ and $f_{\mathrm{Han}}[k]$ with β of 0.6. In test signals D, all methods differed from each other, except for the distributions of $f_{\mathrm{MP}}[k]$ and $f_{\mathrm{Han}}[k]$ with β of 0.3 and 0.6. In test signals E all differed, except for the distributions of $f_{\mathrm{MP}}[k]$ and $f_{\mathrm{Han}}[k]$ as well as $f_{\mathrm{MP}}[k]$ and $f_{\mathrm{HTLS}}[k]$ with β of 0.3 and 0.6.

In test signals A and B there was the dominant spindle and background activity only. Looking at mean error, the HTLS method was very good with sinusoidal background (test signals A) but quite comparable to the other methods with noise background (test signals B), where matching pursuit provided best results. The different backgrounds caused relatively same level of mean error in frequency determination.

In test signals C–E there was also the second spindle activity, with the relative amplitude specified by β. With small value of β the task of finding the frequency of the dominant spindle was easier and the mean errors were typically lower than with large value of β. The HTLS method provided best results, especially when background was ignored (test signals C) or modeled as sinusoids (test signals D) but also with noise background (test signals E), especially with large β. The matching pursuit and zero padded DFT with Hanning windowing were the second best methods. DFT with no zero padding and wavelet method provided poor results overall.

The values of confusion were small in methods providing most accurate spindle frequency values, while in DFT with no zero padding they were largest.

Considering then the test signal set II with waxing and waning spindle pattern. In all test signals (and with both values of β), the distributions of dominant spindle frequency values of all methods were statistically significantly different from each other except for the distributions of $f_{\mathrm{MP}}[k]$ and $f_{\mathrm{Han}}[k]$.

In test signals A and B, the MP method provided best results, followed closely by zero padded DFT with Hanning windowing while HTLS method was clearly poorer than in set I.

In test signals C and D, with small value of β the mean errors were typically lower than with large value of β, as in set I. The MP method provided best results also here, except in C, where zero padded DFT with Hanning windowing was the most accurate method.

4. Discussion

In the present work, we attempted to find the dominant spindle frequency employing different methods often used in the analysis of sleep EEG and other bio-signals. Simulated spindle activity with known frequency content was studied as it offered a way for quantitative analysis of spindle frequency determination results. This is because, naturally, the true frequencies of true EEG sleep spindles are not known.

We formed the simulated test signals with spindle activities and the background. The waxing and waning pattern of spindles is mostly observed in real spindle waveforms, however, with a large variability in appearance. The simulated dominant spindle activity of waxing and waning amplitude had a duration and pattern of the shortest real spindle which is 0.5 s. The simulated 0.5 s dominant spindle activity of constant amplitude envelope can be assumed to represent the middle part of the longest possible spindle. Therefore, the two extreme points were modeled, between which all real spindles can be assumed to fit reasonably well. The background EEG activities were modeled in two ways, as small sinusoids spread across the spindle frequency range and as noise signals containing all frequencies in the same range.

Table 2
Mean error $\bar{\Delta}$ (Hz) and confusion $\bar{c}$ of dominant spindle frequency determination of set II, median values resulting from 100 Monte-Carlo realizations are given

Test signal type, additional components	β	Matching pursuit		DFT, Hanning windowing and zero padding		DFT, Hanning windowing and no zero padding		Wavelet		HTLS	
		$\bar{\Delta}$	$\bar{c}$	$\bar{\Delta}$	$\bar{c}$	$\bar{\Delta}$	$\bar{c}$	$\bar{\Delta}$	$\bar{c}$	$\bar{\Delta}$	$\bar{c}$
A, SinBack	–	**0.15**	0.02	0.16	0.68	1.0	2.74	1.0	0.37	0.79	0.76
B, NoiseBack	–	**0.13**	0.02	0.14	0.67	1.0	2.75	1.0	0.37	0.73	0.79
C, OtherSpi	0.3	0.21	0.03	**0.20**	0.66	1.0	2.84	1.0	0.38	0.78	0.72
C, OtherSpi	0.6	**0.37**	0.11	0.42	0.60	1.0	2.58	1.08	0.45	0.99	0.62
D, OtherSpi + SinBack	0.3	**0.25**	0.05	0.26	0.65	1.0	2.56	1.01	0.40	0.81	0.70
D, OtherSpi + SinBack	0.6	**0.41**	0.13	0.45	0.80	1.0	2.41	1.09	0.46	0.97	0.62
E, OtherSpi + NoiseBack	0.3	**0.23**	0.05	0.25	0.64	1.0	2.65	1.0	0.40	0.80	0.73
E, OtherSin + NoiseBack	0.6	**0.40**	0.12	0.44	0.73	1.0	2.46	1.08	0.45	0.87	0.62

All test signals A–E contained the dominant waxing and waning spindle activity of 13 Hz. Additional signal components were sinusoidal background, noise background, other spindle and combinations of these, β is the relative magnitude of the other spindle activity. The smallest mean error in each test signal type is marked in bold.

The first one was a simpler version of background activities and the latter a more realistic one. The waveform interference was considerable in all used test signals (Fig. 2).

With the present MP code vectors it was certain that the MP method, which can ideally have all waveforms in its code dictionary, now had the optimal waveform shapes available and we could see how well they would perform with respect to each other methods, which included sinusoidal-like code vectors and other smooth waveforms. With DFT and zero padding frequency resolution of 0.1 Hz was obtained, although the test signals were so short. Although the fundamental frequency resolution of the amplitude spectra was not increased, as described by Kay and Marple (1981), the DFT method with zero padding performed interestingly well so that the mean error almost similar to the MP method was achieved. Only in test signal set I, MP was statistically significantly more accurate method of these two. With no zero padding in the DFT method, the frequency resolution was as coarse as 2 Hz with the 0.5 s test signals, with bins located at 10, 12, 14 and 16 Hz in spindle frequency range. This provided quite poor results. Therefore, the zero padding did improve the DFT-based frequency analysis considerably. Also, the values of estimated dominant spindle frequency values with these two methods were virtually identical, as illustrated in Fig. 4. This can be explained by the fact that both these methods used very redundant sinusoidal components in signal analysis. The level of redundancy was by far greater than in the wavelet method or DFT with no zero padding. In additional testing, also DFT with rectangular windowing with zero padding was tested. It provided somewhat better results than Hanning in set I but in set II it was worse.

Due to the nature of the test signals used in the present paper, the performance of the WP dictionary was expected to be relatively poor. However, WP could be a suitable approach if our EEG analysis windows become longer and the spindles do not spread across the whole duration of the analysis epoch. There was no issue of time-localization in the present work as we studied short signal segments of 0.5 s that were totally occupied with spindle activity. This segment length was deliberately selected so, to be in concordance with our previous studies on real EEG spindles, for instance (Himanen et al., 2003; Huupponen et al., 2000, 2003). One can use multiple 0.5 s signal segments with, for example, 80% overlapping, to process all-night EEG traces.

Due to the underlying exponentially damped sinusoidal (EDS) model, HTLS is especially designed to analyse sinusoidal signals. This explains the good results obtained on the (A, C, D) simulation signals of set I (with sinusoidal background). Somewhat worse results are obtained when the signal under analysis does not fit completely to the EDS model. This is reflected in the worse results of B compared to A, and E compared to D. Filtered Gaussian noise (non-sinusoidal) background was added in B and E, which causes a deviation from the EDS model. However, even in these cases the obtained results are comparable or even better than the results obtained by the other methods (MP and DFT). However, the EDS model is not an appropriate model to model the Gaussian modulation of the sinusoids in the waxing and waning simulated signals of set II. Exponentially damped sinusoids with frequencies different than the true frequencies are used to model sinusoids with Gaussian amplitude modulation. As a consequence, much worse results on the dominant frequency determination are obtained as shown in Table 2. Since the waxing and waning is a characteristic property of sleep spindles, these poor results rise some questions on the use of HTLS for the dominant frequency determination of sleep spindles in real practice.

The main point of the present work was to study the capabilities of the five methods to provide accurate spindle frequencies, irrespective of their computational demands. An accurate method could be justified a higher computational load, of course. Computational load of DFT is light, $O(m^2)$, where m is the length of the (zero padded) signal segment (FFT is even lighter, $O(m \times \log(m))$). The computational load related to MP analysis is large, $O(k \times n)$, where k is the number of code vectors used and n is the length of each code vector. The computational load of HTLS is $O(p^3)$ where p is half the length of the signal segment without zero padding. This load is high due to the computation of a full singular value decomposition (Van Huffel et al., 1994). However, the latter computation can be avoided by using a rank-revealing ULV decomposition (Vanhamme et

al., 1998) or Lanczos methods with partial re-orthogonalization (Laudadio et al., 2002), thereby reducing the computational load to $O(p^2)$. The processing speed of the wavelet-based estimation is comparable to that of the DFT methods.

We have found no previous studies in the literature where attention would have been given to the accuracy of the frequency determination is investigated for spindles. We find this necessary as otherwise perhaps too optimistic impression of the methods and results may be given. With real EEG it is naturally very difficult to quantify this aspect. We tried to shed some light to this matter here. Most real spindles, perhaps 90–95% of them seem to consist of one dominant spindle activity and background activity (Zygierewicz et al., 1999; Huupponen et al., 2005b). It seems that in such spindles (test signals A and B) as well as spindles consisting of two spindle activities, perhaps 5–10% of true spindles (test signals C–E), MP and DFT with zero padding performed well overall, also with waxing and waning spindle pattern, and seem to be the most reliable methods of those compared here.

Acknowledgements

This study was financially supported by the BIOPATTERN EU Network of Excellence, EU Contract 508803, the Academy of Finland, project No 44876 (Finnish Centre of Excellence Program, 2000–2005), the National Technology Agency of Finland project Microsleep (“Analysis method of studying the microstructure of sleep”, 2003–2005), the “Programmatorische Federale Overheidsdienst Wetenschapsbeleid” of the Belgian Government, and the FWO through project G.0360.05 (“EEG signal analysis for epilepsy monitoring”).

References

Akin A, Akgül T. Detection of sleep spindles by discrete wavelet transform. In: Proceedings of the 24th IEEE Annual Northeast Bioengineering Conference; 1998. p. 15–7.

De Clercq W, Lemmerling P, Vanrumste B, Van Paesschen W, Van Huffel S. Analyzing multichannel scalp electroencephalograms of patients with epilepsy using exponential data modeling. In: Proceedings of the Second International Conference on Advances in Medical Signal and Information Processing (MEDSIP2004); 2004. p. 104–9.

Gondenck AR, Smith JR. Dynamics of human sleep sigma spindles. Electroenceph Clin Neurophysiol 1974;37:293–7.

Hasan J. Past and future of computer-assisted sleep analysis and drowsiness assessment. J Clin Neurophysiol 1996;13(4):295–313.

Himanen S-L, Virkkala J, Huhtala H, Hasan J. Spindle frequencies in sleep EEG show U-shape within first four NREM sleep episodes. J Sleep Res 2002;11:35–42.

Himanen S-L, Virkkala J, Huupponen E, Hasan J. Spindle frequency remains slow in sleep apnea patients throughout the night. Sleep Med 2003;4(4):361–6.

Huupponen E, Värri A, Hasan J, Himanen S-L, Lehtokangas M, Saarinen J. Optimization of sigma amplitude threshold in sleep spindle detection. J Sleep Res 2000;9(4):327–34.

Huupponen E, Himanen S-L, Hasan J, Värri A. Automatic analysis of electroencephalogram sleep spindle frequency throughout the night. Med Biol Eng Comp 2003;41(6):727–32.

Huupponen E, Saastamoinen A, Niemi J, Virkkala J, Hasan J, Värri A, et al. Automated frequency analysis of synchronous and diffuse sleep spindles. Neuropsychobiology 2005a;51(4):256–64.

Huupponen E, Saastamoinen A, Virkkala J, Himanen S-L, Hasan J, Värri A. Determination of EEG sleep spindle frequency with DFT and matching pursuit approaches. In: Proceedings of the BioMED2005; 2005b. p. 383–6.

Jankel WR, Niedermeyer E. Sleep spindles. J Clin Neurophysiol 1985;2(1):1–35.

Kay SM, Marple SL. Spectrum analysis—a modern perspective. Proceedings of the IEEE 1981;69:1380–419.

Laudadio L, Mastronardi N, Vanhamme L, Van Hecke P, Van Huffel S. Improved Lanczos algorithms for blackbox MRS data quantitation. J Magn Res 2002;157:292–7.

Lemmerling P. Structured total least squares: analysis, algorithms and applications. PhD Thesis, Department of Electrical Engineering, 1999; Katholieke Universiteit Leuven, Leuven, Belgium.

Mallat SG, Zhang Z. Matching pursuit with time–frequency dictionaries. IEEE Trans Sig Proc 1993;41:3397–415.

Morren G, Van Huffel S, Helon I, Naulaers G, Daniels H, Devlieger H, et al. Effects of non- nutritive sucking on heart rate, respiration, and oxygenation: a model-based signal processing approach. Comp Biochem Physiol 2002;132:97–106.

Naitoh P, Antony-Baas V, Muzet A, Ehrhart J. Dynamic relation of sleep spindles and K-komplexes to spontaneus phasic arousals in sleeping human subjects. Sleep 1982;5:58–72.

Papy JM, De Lathauwer L, Van Huffel S, A shift invariance-based order selection technique for the exponential data modeling. Internal Report 05-130, 2005, ESAT-SISTA. Leuven, Belgium: K.U. Leuven. Submitted for publication.

Penzel T, Conradt R. Computer-based sleep recording and analysis. Sleep Med Rev 2000;4(2):131–48.

Schimicek P, Zeitlhofer J, Anderer P, Saletu B. Automatic sleep-spindle detection procedure: aspects of reliability and validity. Clin Electroenceph 1994;25(1):26–9.

Siegel S. Nonparametric statistics for the behavioral sciences. McGraw-Hill Book Company Inc; 1956.

Uchida S, Maloney T, Feinberg I. Sigma (12–16 Hz) and beta (20–28 Hz) EEG discriminate NREM and REM sleep. Brain Res 1994;659:243–8.

Van Huffel S, Chen H, Decanniere C, Van Hecke P. Algorithm for time-domain NMR data fitting based on total least squares. J Magn Res A 1994;110:228–37.

Vanhamme L, Fierro R, Van Huffel S, De Beer R. Fast removal of residual water in proton spectra. J Magn Res 1998;132:197–203.

Werth E, Achermann P, Dijk D-J, Borbely AA. Spindle frequency activity in the sleep EEG: individual differences and topographic distribution. Electroenceph Clin Neurophysiol 1997;103:535–42.

Zeitlhofer J, Gruber G, Anderer P, Asenbaum S, Schimicek P, Saletu B. J Sleep Res 1997;6(3):149–55.

Zygierewicz J, Blinowska KJ, Durka PJ, Szelenberger W, Niemcewicz S, Androsiuk W. High resolution study of sleep spindles. Clin Neurophysiol 1999;110:2136–47.